Optically detected magnetophonon resonances in semiconductor based *n*-Ge and *n*-GaAs

S. Y. Choi,[1] S. C. Lee,[1] H. J. Lee,[2] H. S. Ahn,[3] S. W. Kim,[4] and J. Y. Ryu[1]
[1]*Department of Physics, Cheju National University, Cheju 690–756, Korea*
[2]*Department of Physics, Kyungpook National University, Taegu 702–701, Korea*
[3]*Department of Applied Physics, Korea Maritime University, Pusan 606-791, Korea*
[4]*Department of Physics, Andong National University, Andong 760–749, Korea*
(Received 13 October 2001; revised manuscript received 27 June 2002; published 29 October 2002)

We apply the frequency-dependent magnetoconductivity presented previously by one of the present authors not only to bulk nonpolar (*n*-Ge) and polar (*n*-GaAs) semiconductors but also to short-period Ge-based (nonpolar) and GaAs-based (polar) semiconductor superlattices. We also obtain the optically detected magnetophonon resonance (ODMPR) conditions and the energy range in which the relaxation rates are allowed. With the ODMPR conditions and the obtained energy range, qualitative features of the ODMPR effects are investigated according to the incident photon frequency and the strength of the applied magnetic field in the quantum limit condition, in which $\hbar\omega_c \gg k_B T$ are satisfied. In particular, anomalous behaviors of the ODMPR lineshape such as the splitting and the shift of ODMPR peaks are discussed. Furthermore, the appearance of the plateau between neighboring ODMPR peaks, the disappearance of ODMPR peaks, and changes in the ODMPR amplitude in the semiconductor superlattices are discussed in detail.

DOI: 10.1103/PhysRevB.66.155208 PACS number(s): 73.21.−b, 73.40.−c, 72.20.Dp

I. INTRODUCTION

Magnetophonon resonance (MPR) arises from an electron resonant scattering due to absorption and emission of phonons when the energy separation between two of the Landau levels is equal to a phonon energy. Since the work by Gurevich and Firsov,[1] this effect has been extensively studied as a powerful spectroscopic tool for investigating transport behavior of electrons in bulk[2,3] and low-dimensional semiconductor systems.[4–14] The MPR enables us to obtain information on band structure parameters, such as the effective mass and the energy levels, and on the electron-phonon interaction. The vast majority of work on the MPR has been done on the transport properties of semiconductors, usually the magnetoresistance, which inevitably involves a complicated average of scattering processes. The oscillations in the magnetoresistance are the results of a combination of scattering and broadening processes that can lead to a quite complicated dependence of the resonance amplitudes on doping, sample structure, carrier concentration, and temperature. However, it is known that the MPR can also be observed directly through a study of the electron cyclotron resonance (CR) linewidth and effective mass, i.e., the so-called optically detected MPR (ODMPR), as was demonstrated in three-dimensional (3D) semiconductor systems of GaAs by Hai and Peeters[14] and in two-dimensional (2D) semiconductor systems of $GaAs/Al_xGa_{1-x}As$ heterojunctions by Barnes *et al.*[15] The ODMPR allows one to make quantitative measurements of the scattering strength for specific Landau levels and yields direct information on the nature of the electron-phonon interaction in semiconductors.

The purpose of the present work is to apply the frequency-dependent magnetoconductivity[16] obtained by using the Mori-type projection operator technique presented by one of the present authors not only to bulk nonpolar (*n*-Ge) and polar (*n*-GaAs) semiconductors but also to short-period Ge-based (nonpolar) and GaAs-based(polar) semiconductor superlattices, and to investigate the features of the optically detected magnetophonon resonances in such materials applied to terahertz frequency. The rest of the paper is organized as follows: In Sec. II, we present our theoretical formulations of the problem for two cases: (1) the bulk semiconductors with nonpolar and polar properties, and (2) the short-period semiconductor superlattices with nonpolar and polar properties, respectively. Numerical results for the magnetoconductivity of both bulk nonpolar (*n*-Ge) and polar (*n*-GaAs) semiconductors, and Ge-based (nonpolar) and GaAs-based (polar) semiconductor superlattices, respectively, are presented in Sec. III. In particular, the ODMPR conditions for the model systems, and the plateau conditions for the semiconductor superlattices, are given explicitly, and the effect of incident photon frequency and the strength of magnetic field on the ODMPR are discussed. The relaxation rate, which is closely related to ODMPR, is evaluated for the quantum limit condition, assuming that the interaction with a bulk longitudinal-optical (LO) phonon is the dominant scattering mechanism. Here, special attention is given to the anomalous behavior of the ODMPR lineshape, such as the splitting and the shift of ODMPR, the appearance of plateau scattering between the two ODMPR peaks for the semiconductor superlattices, the disappearance of ODMPR peaks, and changes in the ODMPR amplitude. Our results are summarized in the last section.

II. THEORETICAL FRAMEWORK

We consider a system of many noninteracting electrons N_e in interaction with phonons, initially in equilibrium with a temperature T for two cases—the one is a bulk semiconductor with a constant potential energy and the other is a semiconductor superlattices with a periodical potential well in the z direction. Then, in the presence of a static magnetic field directed along the z axis, $\mathbf{B}=(0,0,B)$, the time-independent Hamiltonian H of the system can be written as

 ©2002 The American Physical Society

$$H=H_e+V+H_p=\sum_{\lambda}\sum_{\lambda'}<\lambda|(h_e+v)|\lambda'>a_{\lambda}^{\dagger}a_{\lambda'}+H_p, \tag{1}$$

$$h_e=\frac{1}{2m^*}(\mathbf{p}+e\mathbf{A})^2+U(z), \tag{2}$$

$$v=\sum_{\mathbf{q}}[\gamma_{\mathbf{q}}^{\dagger}b_{\mathbf{q}}^{\dagger}+\gamma_{\mathbf{q}}b_{\mathbf{q}}], \tag{3}$$

$$H_p=\sum_{\mathbf{q}}\hbar\omega_{\mathbf{q}}\left(b_{\mathbf{q}}^{\dagger}b_{\mathbf{q}}+\frac{1}{2}\right), \tag{4}$$

$$\gamma_{\mathbf{q}}=C(\mathbf{q})\exp(i\mathbf{q}\cdot\mathbf{r}), \tag{5}$$

where $|\lambda>$ means the electron state in the conduction band, λ denotes the Landau state $(N,\mathbf{k})$, $N(=0,1,2,\ldots,)$ is the Landau-level index, $a_{\lambda}^{\dagger}$ (a_{λ}) is the creation (annihilation) operator for an electron with effective mass m^* and momentum $\mathbf{p}$, $\mathbf{A}$ denotes the vector potential, $U(z)$, which is a periodical potential well, has zero value in case of the bulk semiconductor, $b_{\mathbf{q}}^{\dagger}$ $(b_{\mathbf{q}})$ is the creation (annihilation) operator for a phonon with momentum $\hbar\mathbf{q}$ and energy $\hbar\omega_{\mathbf{q}}$, $C(\mathbf{q})$ is the interaction operator, and $\mathbf{r}$ is the position vector of an electron. By taking into account the Landau guage of vector potential $\mathbf{A}=(-By,0,0)$, the one-electron normalized eigenfunctions $(<\mathbf{r}|\lambda>)$ and eigenvalues (E_{λ}) in the conduction band are given, respectively, by

$$<\mathbf{r}|\lambda>\equiv<\mathbf{r}|N,k_x,k_z>=\frac{1}{\sqrt{L_x}}\phi_N(y-y_{\lambda})\exp(ik_xx)\xi_{k_z}(z) \tag{6}$$

and

$$E_{\lambda}=E_N(k_z)=(N+1/2)\hbar\omega_c+\varepsilon(k_z)=\varepsilon_N+\varepsilon(k_z) \tag{7}$$

where $y_{\lambda}=-l_B^2k_x$ with $l_B=\sqrt{\hbar/m^*\omega_c}$, k_x is the wave-vector component of the electron in the x direction, $\omega_c(=eB/m^*)$ is the cyclotron frequency in the conduction band, $\phi_N(y)$ in Eq. (6) are the eigenfunctions of the simple harmonic oscillator, and L_x is the x-directional normalization lengths.

For the bulk semiconductor, $\xi_{k_z}(z)$ in Eq. (6) and $\varepsilon(k_z)$ in Eq. (7) are respectively given by

$$\xi_{k_z}(z)=\frac{1}{\sqrt{L_z}}\exp(ik_zz) \tag{8}$$

and

$$\varepsilon(k_z)=\frac{\hbar^2k_z^2}{2m^*}, \tag{9}$$

where k_z is the wave-vector component of the electron in the z direction. The density of states (DOS) is expressed as

$$D(\varepsilon)=2\frac{m^*\omega_cL_xL_yL_z}{2\pi^2\hbar}\sqrt{\frac{m}{2\hbar^2}}\sum_N\frac{\theta(\varepsilon-\varepsilon_N)}{\sqrt{\varepsilon-\varepsilon_N}} \tag{10}$$

where the dimensions of the sample are assumed to be $V=L_xL_yL_z$. $\theta(x)$ is the Heaviside step function defined by $\theta(x)=1$ for $x\geqslant 0$ and $\theta(x)=0$ for $x<0$. This indicates that the DOS diverges at the bottom $(\varepsilon=\varepsilon_N)$ of each subband and decreases as the energy increases.

For the short-period semiconductor superlattice, $\xi_{k_z}(z)$ in Eq. (6) stands for the tight-binding Bloch function in the z direction. The electron energy spectrum of the superlattice, $\varepsilon(k_z)$ in Eq. (7), still forms minibands in the longitudinal direction due to the superlattice periodic potential. In the superlattice layer ($x-y$ plane), however, it is quantized into Landau levels due to the magnetic field. If only the lowest miniband is considered, the electron state can be described, in the Landau representation, by the quantum number N of the Landau level, the wave vector $k_z(-\pi/d_{\mathrm{SL}}<k_z\leqslant\pi/d_{SL})$, and the spin index σ (we neglect the spin-related energy for simplicity). $\varepsilon(k_z)$ means the energy dispersion of the lowest superlattice miniband, which is approximated by a cosine shape under the tight-binding approximation, and is given by[15]

$$\varepsilon(k_z)=\frac{\Delta}{2}(1-\cos k_zd_{SL}), \tag{11}$$

where Δ is the miniband width and d_{SL} denotes the periodicity of the potential. Then, the density of states is expressed as

$$D(\varepsilon)=\frac{m^*\omega_cV}{\pi^2\hbar d_{SL}}\sum_N\frac{1}{\sqrt{(\varepsilon-\varepsilon_N)(\varepsilon_N+\Delta-\varepsilon)}}\times\theta(\varepsilon-\varepsilon_N)\theta(\varepsilon_N+\Delta-\varepsilon), \tag{12}$$

where the dimensions of the sample are assumed to be $V=L_xL_yL_z$. This indicates that the DOS has singular points at the top $(\varepsilon=\varepsilon_N+\Delta)$ and the bottom $(\varepsilon=\varepsilon_N)$ of each miniband.

When a linearly polarized electromagnetic wave of amplitude E and frequency ω is applied for the Faraday configuration $(E\perp B)$ and Voigt configuration $(E\|B)$,[16,17] the absorption power delivered to the system is given as

$$P=(E^2/4)\mathrm{Re}[\sigma_{vv}(\overline{\omega})+\sigma_{vv}(-\overline{\omega})], \tag{13}$$

where Re means "the real part of," $\overline{\omega}=\omega-i\delta(\delta\rightarrow 0^+)$, and $\sigma_{vv}(\overline{\omega})(v=x,\ y,\ \text{or}\ z)$ [or $\sigma_{vv}(-\overline{\omega})$] is the complex optical conductivity corresponding to the right (or left) circularly polarized wave.

A. Optical conductivity in the bulk semiconductor

For the bulk semiconductor, when an electromagnetic wave given by

$$E_x=0,\ E_y=E\cos\omega t,\ E_z=0 \tag{14}$$

is applied along the z axis, and $\sigma_{yy}(\overline{\omega})$ for the Faraday configuration $(E\perp B)$ can be expressed in the linear-response theory as[16,17]

$$\sigma_{yy}(\bar{\omega})=\frac{\hbar}{i\Omega}\sum_{\lambda',\lambda}\frac{f(E_{\lambda'})-f(E_{\lambda})}{E_{\lambda'}-E_{\lambda}}\times\frac{|j_{y\lambda'\lambda}|^2}{\hbar\bar{\omega}-E_{\lambda'}+E_{\lambda}-i\hbar\tilde{\Sigma}_{0\lambda'\lambda}(\bar{\omega})},\qquad(15)$$

where Ω represents the volume of the system, j_y is the y component of the single-electron current operator, $f(E_\lambda)$ is a Fermi-Dirac distribution function associated with the state $|\lambda>$ and the energy E_λ, and the quantity $i\hbar\tilde{\Sigma}_{0\lambda'\lambda}(\bar{\omega})$ means the line shape function, which is responsible for the spectral broadening of line shape. Therefore, the real and imaginary parts of $i\hbar\tilde{\Sigma}_{0fi}(\bar{\omega})$ defined by

$$i\hbar\tilde{\Sigma}_{0\lambda'\lambda}(\bar{\omega})\equiv\hbar\tilde{\nabla}_{0\lambda'\lambda}(\bar{\omega})+i\hbar\tilde{\Gamma}_{0\lambda'\lambda}(\bar{\omega})\qquad(16)$$

are the line shift and linewidth, respectively, for the transition arising from the resonant absorption or emission of a single photon of frequency ω and of a single phonon of frequency $\omega_{\mathbf{q}}$ between states $|\lambda>$ and $|\lambda'>$. Real and imaginary parts of Eq. (16) are of basic interest and are related to the quantities measured experimentally. The real part provides the resonance shifting whereas the imaginary part gives directly the average value of the relaxation time, the inverse of which then measures the resonance broadening of the absorption spectrum.

Now, let us consider the case where the nondegenerate limit and the quantum limit ($\hbar\omega_c\gg k_BT$) are satisfied so that the electrons can be in the lowest Landau levels.

To obtain the magnetoconductivity $\sigma_{yy}(\bar{\omega})$ of Eq. (15) for the model systems given in Eqs. (6) and (7), we use the matrix elements of the y-component single-electron current operator $|\langle Nk_xk_z|j_y|N'k_x'k_z'\rangle|^2$ given by

$$|\langle Nk_xk_z|j_y|N'k_x'k_z'\rangle|^2=(e^2\hbar\omega_c/2m^*)[(N+1)\delta_{N+1N'}+N\delta_{N-1N'}]\delta_{k_x,k_x'}\delta_{k_z,k_z'}\qquad(17)$$

because the matrix element with respect to the current operator in Eq. (17) is directly proportional to the frequency-dependent magnetoconductivity, where the Kronecker symbols ($\delta_{NN'},\delta_{k_x,k_x'},\delta_{k_z,k_z'}$) denote the selection rules, which arise during the integration of the matrix elements with respect to each direction. We also replace summations with respect to k_x and k_z in Σ_{N,k_x,k_z} by the following relation:[7]

$$\sum_{k_x,k_z}(\cdots)=(L_xL_z/4\pi^2)\int_{-m^*\omega_cL_y/2\hbar}^{m^*\omega_cL_y/2\hbar}dk_x\int_{1stBZ}dk_z(\cdots)\qquad(18)$$

because the ranges of k_x and k_z are, respectively, given within $-(m^*\omega_cL_y/2\hbar)\langle k_x\rangle(m^*\omega_cL_y/2\hbar)$ and $-\pi/L_z\langle k_z\rangle\pi/L_z$. In addition, we assume that the f's in Eq. (15) can be replaced by the Boltzmann distribution function for nondegenerate semiconductor,[7] i.e., $f[E_N(k_z)]\approx\exp\{\beta[\mu-E_N(k_z)]\}$, where $\beta=1/k_BT$ with k_B being the Boltzmann constant and T temperature, and μ denotes the chemical potential given by $\mu=(1/\beta)\ln[4\pi^2\hbar^2n_e\sinh(\beta\hbar\omega_c/2)\sqrt{\beta/(2\pi m^{*3}\omega_c^2)}]$. Here $n_e=N_e/\Omega$ denotes the electron density. Then, we obtain the frequency-dependent magnetoconductivity corresponding to the right-circularly polarized wave as

$$\frac{\sigma_{yy}(\bar{\omega})}{\sigma_0}=\sqrt{\frac{\beta}{2\pi m^*\tau_0^2}}\sinh\left(\frac{1}{2}\beta\hbar\omega_c\right)(1-\exp[-\beta\hbar\omega_c])\times\sum_{N=0}^{\infty}(N+1)\exp\left[-\beta\left(N+\frac{1}{2}\right)\hbar\omega_c\right]\times\int_{1stBZ}\exp\left[-\frac{\beta\hbar^2k_z^2}{2m^*}\right]\times\frac{\tilde{\Gamma}_{0N+1,k_x,k_z;Nn,k_x,k_z}(\omega)}{(\hbar\omega-\hbar\omega_c)^2+\tilde{\Gamma}^2_{0N+1,k_x,k_z;N,k_x,k_z}(\omega)}dk_z\qquad(19)$$

for a shift of zero, $\tilde{\nabla}_0\simeq0$, in the spectral line shape, where $\sigma_0=e^2n_e\tau_0/m^*$ with τ_0 being static relaxation time in the absence of a photon.

An analytical expression of the line shape function in Eq. (15) in the lowest-order approximation for the weak electron-phonon interaction can be written by Eq. (4.6) of Ref. 16 as follows:

$$i\hbar\tilde{\Sigma}_{0\lambda+1\lambda}(\bar{\omega})=\sum_{\mathbf{q}}(1+n_{\mathbf{q}})\left[\sum_{\lambda'(\neq\lambda+1)}\frac{(\gamma_{\mathbf{q}})_{\lambda+1\lambda'}\{(\gamma_{\mathbf{q}}^+)_{\lambda'\lambda+1}-(\gamma_{\mathbf{q}}^+)_{\lambda'-1\lambda}j_{y\lambda'\lambda'-1}/j_{y\lambda+1\lambda}\}}{\hbar\bar{\omega}-E_{\lambda'}+E_{\lambda}-\hbar\omega_{\mathbf{q}}}+\sum_{\lambda'(\neq\lambda)}\frac{\{(\gamma_{\mathbf{q}})_{\lambda\lambda'}-(\gamma_{\mathbf{q}})_{\lambda+1\lambda'+1}j_{y\lambda'+1\lambda'}/j_{y\lambda+1\lambda}\}(\gamma_{\mathbf{q}}^+)_{\lambda'\lambda}}{\hbar\bar{\omega}-E_{\lambda+1}+E_{\lambda'}+\hbar\omega_{\mathbf{q}}}\right]+\sum_{\mathbf{q}}n_{\mathbf{q}}\left[\sum_{\lambda'(\neq\lambda+1)}\frac{(\gamma_{\mathbf{q}}^+)_{\lambda+1\lambda'}\{(\gamma_{\mathbf{q}})_{\lambda'\lambda+1}-(\gamma_{\mathbf{q}})_{\lambda'-1\lambda}j_{y\lambda'\lambda'-1}/j_{y\lambda+1\lambda}\}}{\hbar\bar{\omega}-E_{\lambda'}+E_{\lambda}+\hbar\omega_{\mathbf{q}}}\times\sum_{\lambda'(\neq\lambda)}\frac{\{(\gamma_{\mathbf{q}}^+)_{\lambda\lambda'}-(\gamma_{\mathbf{q}}^+)_{\lambda+1\lambda'+1}j/j_{y\lambda+1\lambda}\}(\gamma_{\mathbf{q}})_{\lambda'\lambda}}{\hbar\bar{\omega}-E_{\lambda+1}+E_{\lambda'}-\hbar\omega_{\mathbf{q}}}\right],\qquad(20)$$

where $n_{\mathbf{q}}$ is the optical-phonon distribution function given by $[\exp(\beta\hbar\omega_{\mathbf{q}})-1]^{-1}$. Equation (20) is identical with Choi *et al.*'s result[17] obtained by Argyres-Sigel's projection operator method[18] in the cyclotron resonance transition problem. Equation (20) is good for sufficiently weak scattering which neglects the many-body coherence effect. The explicit expression of linewidth can be evaluated from Eqs. (16) and (20) by taking the imaginary part of the line shape given in Eq. (20), which is given by

$$
\begin{aligned}
[\tilde{\Gamma}_{0\lambda+1\lambda}(\omega)]_{ph} &\equiv \mathrm{Im}\{i\hbar\tilde{\Sigma}_{0\lambda+1\lambda}(\overline{\omega})\} \\
&= \pi\sum_{\mathbf{q}}(1+n_{\mathbf{q}})\Bigg[\sum_{\lambda'(\neq\lambda+1)}(\gamma_{\mathbf{q}})_{\lambda+1\lambda'}\{(\gamma_{\mathbf{q}}^{\dagger})_{\lambda'\lambda+1}-(\gamma_{\mathbf{q}}^{\dagger})_{\lambda'-1\lambda}j_{y\lambda'\lambda'-1}/j_{y\lambda+1\lambda}\}\times\delta(\hbar\omega-E_{\lambda'}+E_{\lambda}-\hbar\omega_{\mathbf{q}}) \\
&\quad+\sum_{\lambda'(\neq\lambda)}\{(\gamma_{\mathbf{q}})_{\lambda\lambda'}-(\gamma_{\mathbf{q}})_{\lambda+1\lambda'+1}j_{y\lambda'+1\lambda'}/j_{y\lambda+1\lambda}\}(\gamma_{\mathbf{q}}^{\dagger})_{\lambda'\lambda}\times\delta(\hbar\omega-E_{\lambda+1}+E_{\lambda'}+\hbar\omega_{\mathbf{q}}) \\
&\quad+\sum_{\mathbf{q}}n_{\mathbf{q}}\Bigg[\sum_{\lambda'(\neq\lambda+1)}(\gamma_{\mathbf{q}}^{\dagger})_{\lambda+1\lambda'}\{(\gamma_{\mathbf{q}})_{\lambda'\lambda+1}-(\gamma_{\mathbf{q}})_{\lambda'-1\lambda}j_{y\lambda'\lambda'-1}/j_{y\lambda+1\lambda}\}\times\delta(\hbar\omega-E_{\lambda'}+E_{\lambda}+\hbar\omega_{\mathbf{q}}) \\
&\quad+\sum_{\lambda'(\neq\lambda)}\{(\gamma_{\mathbf{q}}^{\dagger})_{\lambda\lambda'}-(\gamma_{\mathbf{q}}^{\dagger})_{\lambda+1\lambda'+1}j/j_{y\lambda+1\lambda}\}(\gamma_{\mathbf{q}})_{\lambda'\lambda}\times\delta(\hbar\omega-E_{\lambda+1}+E_{\lambda'}-\hbar\omega_{\mathbf{q}})\Bigg],
\end{aligned}
\tag{21}
$$

where the symbol Im in Eq. (21) denotes the imaginary parts of the quantity. The line shift, $\hbar\tilde{\nabla}_{0\lambda+1\lambda}(\omega)$ $[\equiv\mathrm{Re}\{i\hbar\tilde{\Sigma}_{0\lambda+1\lambda}(\overline{\omega})\}]$, can be calculated through a Kramers-Kronig relation:

$$
\tilde{\nabla}_0(\omega)=\frac{1}{\pi}\mathcal{P}\int_{-\infty}^{\infty}\frac{\tilde{\Gamma}_0(\omega')}{\omega-\omega'}d\omega', \tag{22}
$$

where $\tilde{\Gamma}_0(\omega')$ is given by Eq. (21). To obtain Eq. (21), we have used the Dirac identity $\lim_{s\to 0^+}(x\pm is)=\mathcal{P}(1/x)\mp i\pi\delta(x)$, where $\mathcal{P}$ denotes Cauchy's principle-value integral.

The matrix elements of $|(\gamma_{\mathbf{q}})_{\lambda\lambda'}|^2$ in Eq. (21) are given in the representation of Eq. (6) by

$$
|(\gamma_{\mathbf{q}})_{\lambda\lambda'}|^2=|C(\mathbf{q})|^2|J_{N,N'}(u_{\perp})|^2\delta_{k_x,k_x'+q_x}\delta_{k_z,k_z'+q_z}, \tag{23}
$$

where the δ functions ensure momentum conservation in the x and z directions in scattering events and

$$
|J_{N,N'}(u_{\perp})|^2=\frac{N_<!}{N_>!}\exp[-u_{\perp}]u_{\perp}^{\Delta N}[L_{N_<}^{\Delta N}(u_{\perp})]^2 \tag{24}
$$

with $u_{\perp}=l_B^2q_{\perp}^2/2$ with $q_{\perp}^2=q_x^2+q_y^2$. Here, $N_<=\min\{N,N'\}$, $N_>=\max\{N,N'\}$, and $L_{N_<}^{\Delta N}(u_{\perp})$ is an associated Laguerre polynomial[19] with $\Delta N=N_>-N_<$. With the help of Eqs. (7) and (23), we obtain the relaxation rate associated with the electronic transition between the states $|\lambda+1>$ and $|\lambda>$ as

$$
\begin{aligned}
[\tilde{\Gamma}_{0\lambda+1\lambda}(\omega)]_{ph} &\approx \pi\sum_{\mathbf{q}}\sum_{N'\neq N+1}|C(\mathbf{q})|^2|J_{N+1,N'}(q_{\perp})|^2\times\{(1+n_{\mathbf{q}})\delta[\hbar\omega-E_{N'}(k_z-q_z)+E_N(k_z)-\hbar\omega_{\mathbf{q}}] \\
&\quad+n_{\mathbf{q}}\delta[\hbar\omega-E_{N'}(k_z+q_z)+E_N(k_z)+\hbar\omega_{\mathbf{q}}]\}+\pi\sum_{\mathbf{q}}\sum_{N',k_x',k_z'\neq N,k_x,k_z}|C(\mathbf{q})|^2|J_{N,N'}(q_{\perp})|^2 \\
&\quad\times\{(1+n_{\mathbf{q}})\delta[\hbar\omega+E_{N'}(k_z+q_z)-E_{N+1}(k_z)+\hbar\omega_{\mathbf{q}}]+n_{\mathbf{q}}\delta[\hbar\omega+E_{N'}(k_z-q_z)-E_{N+1}(k_z)-\hbar\omega_{\mathbf{q}}]\}.
\end{aligned}
\tag{25}
$$

It is interesting to note that the δ-functions in Eqs. (21) and (25) express the law of energy conservation in one-phonon collision (emission and absorption) processes. The energy-conserving δ functions imply that when an electron undergoes a collision by absorbing the energy from the incident photon, its energy can only change by an amount equal to the energy of a phonon involved in the transition. This in fact leads to the optically detected magnetophonon resonance.

To calculate the relaxation rates $\tilde{\Gamma}_0$ of Eq. (25) for electron-phonon interactions, we consider the Fourier component of the interaction potentials[7] for nonpolar optical phonon scattering given by $|C(\mathbf{q})|^2=D/\Omega$ with D being the constant of the nonpolar interaction and for polar LO-phonon scattering given by $|C(\mathbf{q})|^2=D'/(\Omega q^2)$ with D' being the constant of the polar interaction, where the assumption that

the phonons are dispersionless (i.e., $\hbar\omega_{\vec{q}} \approx \hbar\omega_{LO} \approx$ constant, where ω_{LO} is the optical phonon frequency) was made. Then, the relaxation rates associated with the electronic transition between the states $|N+1,k_x,k_z>$ and $|N,k_x,k_z>$ can be expressed for nonpolar and polar optical phonon scatterings, respectively, by

$$\tilde{\Gamma}_0(N+1,k_x,k_z:N,k_x,k_z)=\frac{\sqrt{m^*}D}{2\sqrt{2}\pi\hbar l_B^2}\sum_{N'\neq N}\left\{(n_{\mathbf{q}}+1)\left(\frac{\theta[\Theta_1(k_z)]}{\sqrt{\Theta_1(k_z)}}+\frac{\theta[\Theta_3(k_z)]}{\sqrt{\Theta_3(k_z)}}\right)+n_{\mathbf{q}}\left(\frac{\theta[\Theta_2(k_z)]}{\sqrt{\Theta_2(k_z)}}+\frac{\theta[\Theta_4(k_z)]}{\sqrt{\Theta_4(k_z)}}\right)\right\}, \tag{26}$$

$$\tilde{\Gamma}_0(N+1,k_x,k_z:N,k_x,k_z)=\frac{D'}{4\pi}\sqrt{\frac{m^*}{2\hbar^2}}\sum_{N'\neq N}\sum_{\pm}\left\{(n_{\mathbf{q}}+1)\times\left(K_1^{\pm}(N,N';k_z)\frac{\theta[\Theta_1(k_z)]}{\sqrt{\Theta_1(k_z)}}+K_3^{\pm}(N,N';k_z)\frac{\theta[\Theta_3(k_z)]}{\sqrt{\Theta_3(k_z)}}\right)\right.$$
$$\left.+n_{\mathbf{q}}\left(K_2^{\pm}(N,N';k_z)\frac{\theta[\Theta_2(k_z)]}{\sqrt{\Theta_2(k_z)}}+K_4^{\pm}(N,N';k_z)\frac{\theta[\Theta_4(k_z)]}{\sqrt{\Theta_4(k_z)}}\right)\right\}, \tag{27}$$

where $\omega_{\mathbf{q}}=\omega_{LO}$, $\theta(x)$ is the Heaviside step function,

$$\Theta_1(k_z)=\hbar\omega+(N-N')\hbar\omega_c+\frac{\hbar^2k_z^2}{2m^*}-\hbar\omega_{LO}, \tag{28a}$$

$$\Theta_2(k_z)=\hbar\omega+(N-N')\hbar\omega_c+\frac{\hbar^2k_z^2}{2m^*}+\hbar\omega_{LO}, \tag{28b}$$

$$\Theta_3(k_z)=\hbar\omega+(N'-N-1)\hbar\omega_c-\frac{\hbar^2k_z^2}{2m^*}+\hbar\omega_{LO}, \tag{28c}$$

$$\Theta_4(k_z)=\hbar\omega+(N'-N-1)\hbar\omega_c-\frac{\hbar^2k_z^2}{2m^*}-\hbar\omega_{LO}, \tag{28d}$$

and

$$K_1^{\pm}(N,N';k_z)=\frac{1}{2}\int_0^{\infty}du_{\perp}|J_{N+1,N'}(u_{\perp})|^2\frac{1}{u_{\perp}+a_{1\pm}^2}, \tag{29a}$$

$$K_2^{\pm}(N,N';k_z)=\frac{1}{2}\int_0^{\infty}du_{\perp}|J_{N+1,N'}(u_{\perp})|^2\frac{1}{u_{\perp}+a_{2\pm}^2}, \tag{29b}$$

$$K_3^{\pm}(N,N';k_z)=\frac{1}{2}\int_0^{\infty}du_{\perp}|J_{N,N'}(u_{\perp})|^2\frac{1}{u_{\perp}+a_{3\pm}^2}, \tag{29c}$$

$$K_4^{\pm}(N,N';k_z)=\frac{1}{2}\int_0^{\infty}du_{\perp}|J_{N,N'}(u_{\perp})|^2\frac{1}{u_{\perp}+a_{4\pm}^2}, \tag{29d}$$

with $a_{i\pm}^2=l_B^2(k_z\pm\sqrt{2m^*\Theta_i(k_z)/\hbar^2})^2/2$. In order to obtain Eqs. (26) and (27), we transformed the sum over $\mathbf{q}$ in Eq. (25) into an integral form in the usual way as $\Sigma_{\mathbf{q}} \rightarrow (V/(2\pi)^3)\int_{-\infty}^{\infty}\int_{-\infty}^{\infty}\int_{1stBZ}dq_xdq_ydq_z$ and used the following property of the Dirac δ function: $\delta[f(x)]=\Sigma_i\delta[x-x_i]/|f'(x_i)|$ with x_i being the roots of $f(x)$. In addition, we utilized the relation $\int_{-\infty}^{\infty}\int_{-\infty}^{\infty}|J_{N,N'}(q_{\perp})|^2dq_xdq_y=2\pi/l_B^2$ in doing the integral over q_x and q_y to obtain Eq. (26). It is clearly seen from Eqs. (26) and (27) that the relaxation rates diverge whenever the conditions $\Theta_i(k_z)=0$ and the arguments $a_{i\pm}^2=0$ in $K_i^{\pm}(N,N';t)$ are satisfied. From these conditions, the relaxation rates [and hence, the frequency-dependent magnetoconductivities $\sigma_{yy}(\bar{\omega})$] for both nonpolar LO-phonon and polar LO-phonon scattering show the same resonant behaviors at $P\hbar\omega_c\pm\hbar\omega=\hbar\omega_{LO}$ ($P\equiv N'-N=1,2,3,\ldots,$). When the ODMPR conditions are satisfied, in the course of scattering events, the electrons in the Landau levels specified by the level index (N) can make transitions to one of the Landau levels (N') by absorbing and/or emitting a photon of energy $\hbar\omega$ during the absorption of a LO phonon of energy $\hbar\omega_{LO}$.

B. Optical conductivity in the semiconductor superlattice

For the semiconductor superlattice, when an electromagnetic wave given by

$$E_x=0,\ E_y=0,\ E_z=E\cos\omega t \tag{30}$$

is applied along the y axis, $\sigma_{zz}(\bar{\omega})$ for the Voigt configuration ($E\|B$) can be expressed in the Kubo formalism as[16]

$$\sigma_{zz}(\bar{\omega})=\frac{\beta e^2\Delta^2d_{\mathrm{SL}}^2}{16\hbar\pi^2l_B^2}\sum_n\int_{-\pi/d_{\mathrm{SL}}}^{\pi/d_{\mathrm{SL}}}dk_z\sin^2(k_zd_{\mathrm{SL}})f[E_N(k_z)]$$
$$\times\{1-f[E_N(k_z)]\}\frac{\tilde{\Gamma}_{N,k_x,k_z:N,k_x,k_z}(\omega)}{(\hbar\omega)^2+\tilde{\Gamma}^2_{N,k_x,k_z:N,k_x,k_z}(\omega)} \tag{31}$$

for the shift zero in the spectral line shape, where $\beta=1/k_BT$ with k_B being Boltzmann constant and T tempera-

ture. Also, N indicates the quantum state, $f[E_N(k_z)]$ is a Fermi-Dirac distribution function associated with the eigenstate $|N,k_x,k_z>$ of Eq. (6) and the energy $E_N(k_z)$ of Eq. (7), and $-e(<0)$ is the electron charge. The quantity $\tilde{\Gamma}(\omega)$ given in Eq. (31), which appears in terms of the collision broadening of the absorption spectrum due to the electron-phonon interaction, play the role of the relaxation rate in the spectral line shape. Note that if the limit of $\omega\rightarrow 0$ is taken in Eq. (31), Eq. (31) reduces to the dc magnetoconductivity related to the MPR obtained in Ref. 13. To obtain the longitudinal magnetoconductivity $\sigma_{zz}(\overline{\omega})$ of Eq. (31) for the model systems, we used the matrix elements of the z-component single-electron current operator $|\langle k_z,k_x,N|j_z|N',k_x',k_z'\rangle|^2$ to be

$$|\langle k_z,k_x,N|j_z|N',k_x',k_z'\rangle|^2 = (e\Delta d_{\mathrm{SL}}\sin(k_z d_{\mathrm{SL}})/2\hbar)^2\delta_{NN'}\delta_{k_x k_{x'}}\delta_{k_z k_{z'}}, \tag{32}$$

since the matrix element with respect to the current operator in Eq. (32) is directly proportional to the longitudinal optical magnetoconductivity, where the Kronecker symbols ($\delta_{NN'}$, $\delta_{k_x k_{x'}}$, $\delta_{k_z k_{z'}}$) denote the selection rules, which arise during the integration of the matrix elements with respect to each direction. We also replaced summations with respect to k_x and k_z in Σ_{N,k_x,k_z} by the following relation:[7,13]

$$\sum_{k_x,k_z}(\cdots)\rightarrow(L_xL_z/4\pi^2)\int_{-m^*\omega_c L_y/2\hbar}^{m^*\omega_c L_y/2\hbar}dk_x\int_{-\pi/d_{\mathrm{SL}}}^{\pi/d_{\mathrm{SL}}}dk_z(\cdots). \tag{33}$$

In addition, to express the longitudinal optical magnetoconductivity of Eq. (31) in simpler forms, we assume that the f's in Eq. (31) are replaced by the Boltzmann distribution function for nondegenerate semiconductors,[7,13] i.e., $f[E_N(k_z)]\approx\exp[\beta(\mu-E_N(k_z)]$, where μ denotes the chemical potential given by

$$\mu=(1/\beta)\ln\{4\pi\hbar n_e d_{SL}\sinh(\beta\hbar\omega_c/2)/ [m^*\omega_c\exp(-\beta\Delta/2)I_0(\beta\Delta/2)]\}.$$

Here $n_e=N_e/V$ denotes the electron density and $I_0(x)$ denotes the modified Bessel function.[19] Equation (31) expresses the Drude term arising from the drift motion of electrons with the localized state through the electron-phonon interaction. As shown in Eq. (31), the electronic transport properties (e.g., electronic relaxation processes, magnetophonon resonances, etc.) in the superlattice can be studied by examining the behavior of $\tilde{\Gamma}(\omega)$ as a function of the relevant physical parameters introduced in the theory. In the following, we shall analyze the relaxation rates in detail in order to get insight into optically detected magnetophonon resonance effects in the model system of the superlattices. An analytical expression of the relaxation rate in the lowest-order approximation for the weak electron–phonon interaction and in the limit of weak electric fields can be evaluated from the general expression of the relaxation rate given by Eq. (4.6) of Ref. 16 as follows:

$$\begin{aligned}\tilde{\Gamma}(N,k_x,k_z;N,k_x,k_z)\approx{}&\pi\sum_{\mathbf{q}}\sum_{N'\neq N}|C(\mathbf{q})|^2|J_{N,N'}(u_\perp)|^2\Big((n_{\mathbf{q}}+1)\\&\times\delta\Big\{\hbar\omega+(N-N')\hbar\omega_c-\frac{\Delta}{2}[\cos k_z d_{SL}-\cos(k_z-q_z)d_{SL}]-\hbar\omega_{\mathbf{q}}\Big\}\\&+n_{\mathbf{q}}\delta\Big\{\hbar\omega+(N-N')\hbar\omega_c-\frac{\Delta}{2}[\cos k_z d_{SL}-\cos(k_z+q_z)d_{SL}]+\hbar\omega_{\mathbf{q}}\Big\}\Big)\\&+\pi\sum_{\mathbf{q}}\sum_{N'\neq N}|C(\mathbf{q})|^2|J_{NN'}(u_\perp)|^2\Big((n_{\mathbf{q}}+1)\times\delta\Big\{\hbar\omega+(N'-N)\hbar\omega_c-\frac{\Delta}{2}[\cos(k_z+q_z)d_{SL}\\&-\cos k_z d_{SL}]+\hbar\omega_{\mathbf{q}}\Big\}+n_{\mathbf{q}}\delta\Big\{\hbar\omega+(N'-N)\hbar\omega_c-\frac{\Delta}{2}[\cos(k_z-q_z)d_{SL}-\cos k_z d_{SL}]-\hbar\omega_{\mathbf{q}}\Big\}\Big).\end{aligned} \tag{34}$$

The δ functions in Eq. (34) express the law of energy conservation in one-phonon collision (absorption and emission) processes. This in fact is related to the oscillatory behavior of the optically detected MPR effects due to the Landau levels.

By the same method, the relaxation rates associated with the electronic transition between the states $|N,k_x,k_z\rangle$ and $|N,k_x,k_z\rangle$ can be expressed[13] for nonpolar and polar optical phonon scatterings, respectively, by

$$\tilde{\Gamma}(N,k_x,k_z;N,k_x,k_z)=\frac{D'}{\pi\Delta d_{SL}l_B^2}\sum_{N'\neq N}\sum_{\nu=1}^{2}\sum_{\pm}(n_{\mathbf{q}}+1/2\pm1/2)\frac{\theta\left[1-\frac{4}{\Delta^2}\Theta_{\nu,\pm}^2(k_z)\right]}{\sqrt{\left[1-\frac{4}{\Delta^2}\Theta_{\nu,\pm}^2(k_z)\right]}}, \tag{35}$$

$$\tilde{\Gamma}(N,k_x,k_z;N,k_x,k_z)=\frac{D}{\pi\Delta d_{SL}}\sum_{N'\neq N}\sum_{\nu=1}^{2}\sum_{\pm}(n_{\mathbf{q}}+1/2\pm1/2)\frac{K_{\nu,\pm}(N,N';k_z)\,\theta\left(1-\frac{4}{\Delta^2}\Theta^2_{\nu,\pm}(k_z)\right)}{\sqrt{\left(1-\frac{4}{\Delta^2}\Theta^2_{\nu,\pm}(k_z)\right)}},\tag{36}$$

where $\omega_{\mathbf{q}}=\omega_{LO}$, the symbol $\pm$ in the summation indicates the phonon emission and absorption processes, respectively, $\theta(x)$ is the Heaviside step function,

$$\Theta_{1,\pm}(t)=-\hbar\omega-(N-N')\hbar\omega_c\pm\hbar\omega_{LO}+\frac{\Delta}{2}\cos t,\tag{37a}$$

$$\Theta_{2,\pm}(t)=\hbar\omega-(N-N')\hbar\omega_c\pm\hbar\omega_{LO}+\frac{\Delta}{2}\cos t,\tag{37b}$$

and

$$\begin{aligned}K_{\nu,\pm}(N,N';t)&=\frac{1}{2}\int_0^\infty du|J_{N,N'}(u_\perp)|^2\frac{1}{u_\perp+a^2_{\nu,\pm}}\\&=\frac{e^{a^2_{\nu,\pm}}}{2(\alpha+N_<)!}\sum_{k=0}^{\infty}\sum_{m=0}^{2k}\frac{(2N_<-2k)!(2k)!}{(N_<-k)!}\\&\quad\times\frac{(-1)^m2^m(2k+2\alpha)!(\alpha+m)!}{(2k-m)!(2\alpha+m)!m!}\\&\quad\times\Gamma(-\alpha-m,a^2_{\nu,\pm}).\end{aligned}\tag{38}$$

Here $a^2_{\nu,\pm}=l_B^2d_{SL}^{-2}[t-\cos^{-1}(2\Theta_{\nu,\pm}(t)/\Delta)]^2/2$ with $t=k_zd_{SL}$, $\alpha=N_>-N_<$, and $\Gamma(a,x)$ is the incomplete γ function[19] defined by $\Gamma(a,x)=\int_x^\infty e^{-t}t^{a-1}dt$. In addition, we utilized the following relation in doing the integral over q_x and q_y: $\int_0^\infty\sqrt{u_\perp}|J_{N'N}(u_\perp)|^2du_\perp=1/l_B^2$, to obtain Eq. (36). It is clearly seen from Eqs. (36) and (37) that the relaxation rates diverge whenever the conditions $1-4\Theta^2_{\nu,\pm}(k_z)/\Delta^2=0$ and the arguments $a^2_{\nu,\pm}=0$ in the incomplete γ function $\Gamma(-\alpha-m,a^2_{\nu,\pm})$ [or $K_{\nu,\pm}(N,N';t)$] are satisfied. From these conditions, the relaxation rates [and hence, the longitudinal optical magnetoconductivities $\sigma_{zz}(\bar{\omega})$] for both nonpolar-LO-phonon and polar-LO-phonon scattering show that the same ODMPR gives the resonance conditions at

$$P\hbar\omega_c=\hbar\omega_{LO}\pm\hbar\omega(P\equiv N'-N=1,2,3,\ldots,).\tag{39}$$

When the ODMPR conditions are satisfied, in the course of scattering events, the electrons in the Landau levels specified by the level index (N) could make transitions to one of the Landau levels (N') by absorbing and/or emitting a photon of energy $\hbar\omega$ during the absorption of a LO phonon of energy $\hbar\omega_{LO}$ as those shown in the bulk semiconductors. We see that Eq. (39) exhibits double peaks around the MPR peaks appearing in the absence of an incident photon and that the positions of these peaks are sensitive to the photon frequency. In addition, from the fact that $1-4\Theta^2_{\nu,\pm}(k_z)/\Delta^2$ are real and positive, we can obtain an energy range in which the relaxation rates are allowed under the following condition:

$$\hbar\omega_{LO}\pm\hbar\omega-\Delta\langle P\hbar\omega_c\langle\hbar\omega_{LO}\pm\hbar\omega+\Delta.\tag{40}$$

Our results for the limit of $\omega\rightarrow0$ reduce to the previous one,[13] and they are identical with the results of Noguchi *et al.*[10] and Gassot *et al.*[12] obtained from the dispersion relation and the density of states of a superlattice under high magnetic fields and from the resonant excitation of electrons by optical phonons. It is to be noted that scatterings with optical modes is possible only within the energy range and that the energy range in which scatterings with optical modes are possible is very sensitive to the miniband width, the incident photon frequency, and the strength of applied magnetic fields.

Equation (31), together with Eqs. (35) and (36), is the basic equation for the ODMPR spectral lineshape, which enables us to analyze ODMPR effects in semiconductors under magnetic fields.

III. NUMERICAL RESULTS AND DISCUSSIONS

In this section we present the numerical results of the frequency-dependent magnetoconductivity formula $\sigma_{yy}(\bar{\omega})$ which is related to the ODMPR for the bulk materials and $\sigma_{zz}(\bar{\omega})$ which is related to the ODMPR for the superlattices.

A. Numerical results in the bulk semiconductors

First, we present the numerical results of $\sigma_{yy}(\bar{\omega})$ in Eq. (19), together with Eqs. (26) and (27). Here special attention is given to the behavior of the ODMPR line shape, such as the appearance of ODMPR peaks and the shift of ODMPR peaks. For our numerical results of Eqs. (19), (26), and (27), the parameters of n-GaAs are taken[20,21] by an effective mass $m^*=0.067\ m_0$ with m_0 being the electron rest mass, a LO-phonon energy $\hbar\omega_{LO}=36.6$ meV, the electron density $n_e=4\times10^{24}\,\mathrm{cm}^{-3}$, and the constant of the polar interaction $D'=1.1558\times10^{-49}\ \mathrm{kg^2m^7s^{-4}}$, whereas those of n-Ge are taken[20,21] by an effective mass $m^*=0.082\ m_0$, a LO-phonon energy $\hbar\omega_{LO}=30.3$ meV, the electron density $n_e=4\times10^{24}\,\mathrm{cm}^{-3}$, and the constant of the nonpolar interaction $D=1.059\times10^{-68}\ \mathrm{kg^2m^7s^{-4}}$. In addition, as many as 21 Landau levels are included in the calculation of the

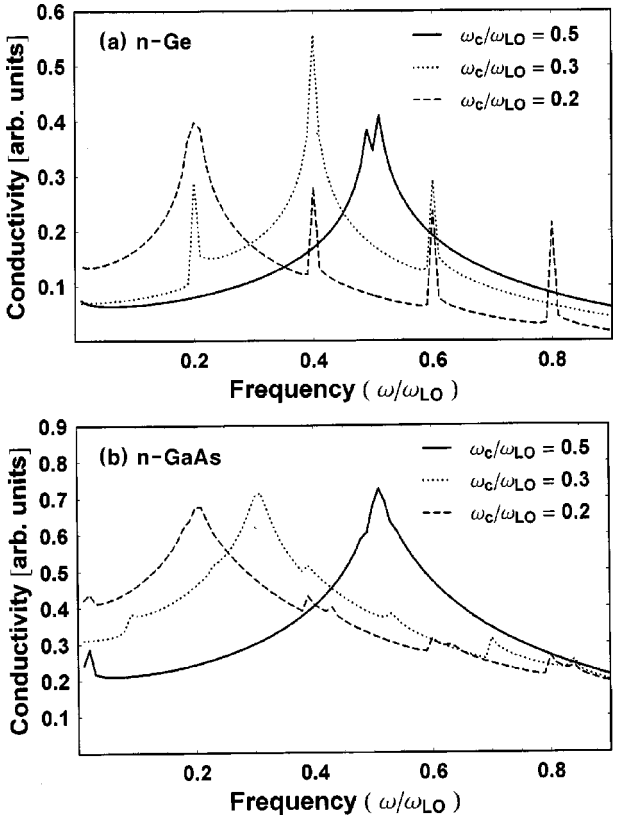

FIG. 1. Magnetic-field dependence of the magnetoconductivity $[\sigma_{yy}(\overline{\omega})]$ as a function of incident photon frequency for (a) *n*-Ge and (b) *n*-GaAs at $T=240$ K. The solid and dashed lines in Fig. 1 are for $\omega_c/\omega_{LO}=0.5$ and 0.2, respectively, and the dotted lines in Figs. 1(a) and 1(b) are for $\omega_c/\omega_{LO}=0.4$ and 0.3, respectively.

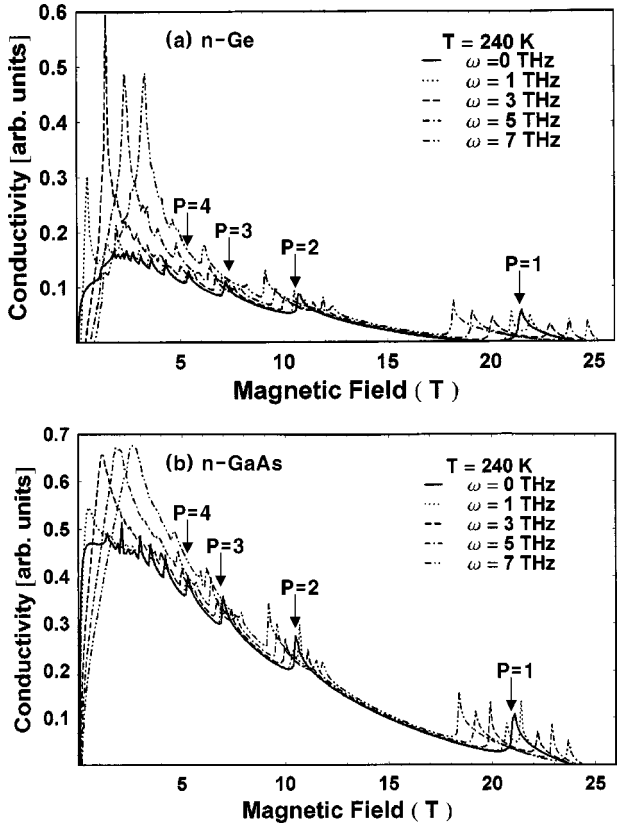

FIG. 2. Photon frequency dependence of the magnetoconductivity $[\sigma_{yy}(\overline{\omega})]$ as a function of applied magnetic field for (a) *n*-Ge and (b) *n*-GaAs at $T=240$ K. The solid, dotted, dashed, dashed-dotted, and dashed-double dotted lines are for $\omega=0,1,3,5$, and 7 THz, respectively.

frequency-dependent magnetoconductivity. The sample temperature is assumed to be 240 K in this calculation.

Figures 1(a) and 1(b) show the magnetic-field strength dependence of the magnetoconductivities $\sigma_{yy}(\overline{\omega})$ for nonpolar material *n*-Ge and polar material *n*-GaAs, respectively, as a function of incident photon frequency. Various peaks are observed according to the incident photon frequency and the strength of the magnetic field. It is clearly seen from the figures that main peaks are observed in terms of the cyclotron resonance condition ($\omega=\omega_c$) and/or the optically detected magnetophonon resonance condition given by $P\hbar\omega_c \pm\hbar\omega=\hbar\omega_{LO}$ ($P\equiv N'-N=1,2,3,\ldots$) whereas subsidiary peaks are exhibited in terms of the optically detected magnetophonon resonance condition. Therefore, it is to be noted that all peaks can be assigned from the CR and the ODMPR condition. Our results for *n*-GaAs material are somewhat different from Hai and Peeters's theoretical results.[14]

Figure 2 shows the incident photon frequency dependence of the magnetoconductivities $\sigma_{yy}(\overline{\omega})$ for (a) nonpolar material *n*-Ge and (b) polar material *n*-GaAs as a function of magnetic field B at $T=240$ K, where various incident photon frequencies ranging from 0 THz to 7 THz are taken in order to investigate the dependence of the ODMPR effect on the incident photon frequency parameters. In these figures, various peaks are observed according to the incident photon frequency. Large peaks in low magnetic field side are observed in terms of cyclotron resonance ($\omega=\omega_c$) and all peaks except for large peaks in low magnetic are exhibited in terms of the optically detected magnetophonon resonance. As mentioned above, our main concern here is the behavior of the ODMPR line shape, such as the appearance of ODMPR peaks and the shift of ODMPR peaks. From the figures we can see the following features: (i) as a linearly polarized photon of amplitude E and frequency ω is incident along the z axis, the splitting of the ODMPR peaks takes place from the MPR peaks, (ii) as the photon frequency is increased, the shifts of the ODMPR peak positions are increased, and (iii) as the difference of Landau-level indices is increased, the MPR and ODMPR peak positions are shifted to the lower magnetic-field side. All features (i), (ii), and (iii) are the same for nonpolar material, and polar material and they can be readily understood from the condition for the ODMPR to give the peak positions (i.e., resonant magnetic fields) in the spectral line shape and are mainly determined by the conditions $\Theta_i(k_z)=0$ and the arguments $a_{i\pm}^2=0$ in Eqs. (26) and (27). The resonant behaviors are actually given by $P\hbar\omega_c \pm\hbar\omega=\hbar\omega_{LO}$ ($P\equiv N'-N=1,2,3,\ldots,$). If there is no photon energy $\hbar\omega$ in the ODMPR condition, it becomes the MPR condition given by $P\hbar\omega_c=\hbar\omega_{LO}$ ($P\equiv N'-N=1,2,3,\ldots,$). Accordingly, we see that the ODMPR peaks

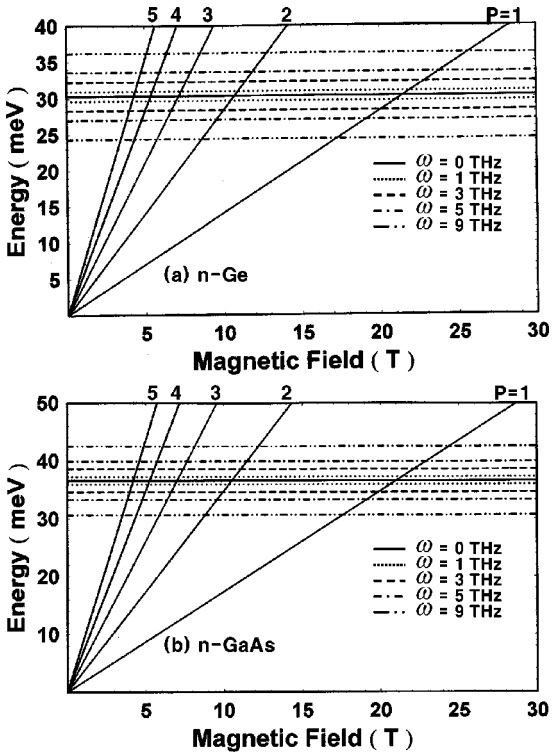

FIG. 3. Energy vs applied magnetic field for various incident photon frequencies in (a) *n*-Ge and (b) *n*-GaAs. The solid, dotted, dashed, dashed-dotted, and dashed-double dotted lines are for $\omega = 0,1,3,5,$ and 9 THz, respectively. Here the crossing points indicate the resonance magnetic field.

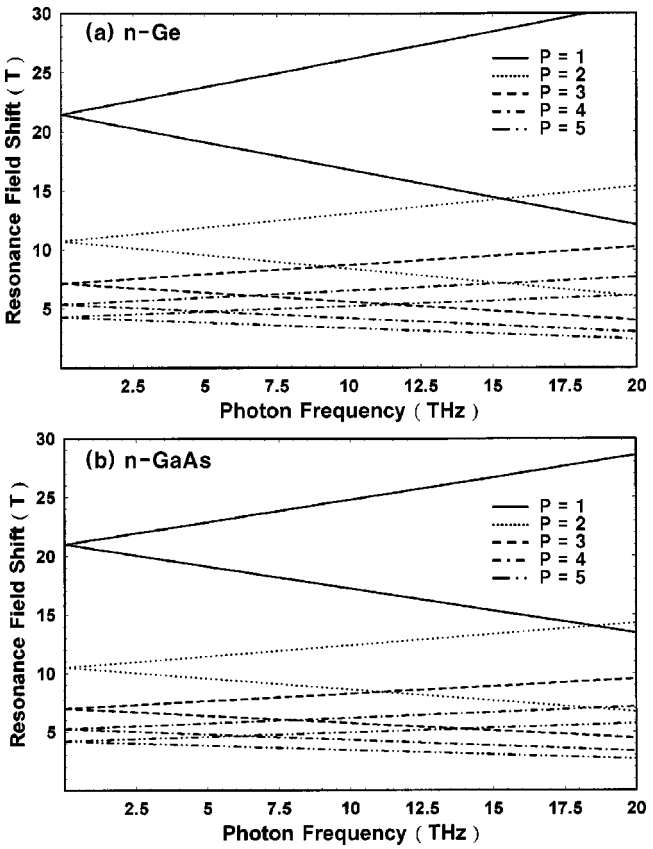

FIG. 4. Dependence of resonance field shift on the incident photon frequency for various transitions in (a) *n*-Ge and (b) *n*-GaAs. The solid, dotted, dashed, dashed-dotted, and dashed-double dotted lines are for $P \equiv N' - N = 1,2,3,4,$ and 5, respectively.

are split from MPR peaks. It seems that this splitting is due to the absorption and emission of a photon during the absorption of a phonon and it is due to the incident photon being linearly polarized because the linearly polarized wave is composed of the superposition of a right-circularly polarized wave and a left-circularly polarized wave. For a fixed phonon energy in the ODMPR condition, as the photon frequency ω is increased, the shift of the resonant magnetic field (via ω_c) is increased, as in feature (ii). In addition, for a fixed photon energy and a fixed phonon energy, the resonant magnetic field is decreased since $P\omega_c$ is constant if the difference in the Landau-level indices is increased, as in feature (iii). Thus it is to be noted that all features (i), (ii), and (iii) shown in Fig. 2 can be understood from the ODMPR condition.

Figure 3 demonstrates the resonant magnetic fields due to each transition for (a) *n*-Ge material and (b) *n*-GaAs material, where all MPR and ODMPR peaks in Fig. 2 are assigned from the crossing point giving the resonant magnetic field in Fig. 3. It is clearly seen from the figure that as the difference of Landau-level indices is increased, the MPR and ODMPR peak positions are shifted to the lower magnetic-field side, as mentioned in feature (iii) of Fig. 2. It is also shown that the shifts of ODMPR are increased as the incident photon frequency is increased and the increase of ODMPR shift is largest in the case of $P=1$. We can get the same resonant magnetic fields due to each transition for the Ge-based superlattices and the GaAs-based superlattices as shown in Fig. 3.

Figure 4 shows the dependence of the ODMPR shifts on the incident photon frequency according to the difference of Landau-level indices. It can be seen from the figure that the shifts of ODMPR are increased as the incident photon frequency is increased and the difference in the Landau level indices is decreased, as expected in Figs. 2 and 3. It is interesting to note that the qualitative behaviors of the ODMPR are the same for nonpolar and polar materials.

B. Numerical results in the semiconductor superlattice

Second, we present the numerical results of $\sigma_{zz}(\overline{\omega})$ in Eq. (31), together with Eqs. (35) and (36). Here special attention is given to the behavior of the ODMPR line shape, such as not only the appearance of ODMPR peaks and the shift of ODMPR peaks as shown in the results of the bulk semiconductors, but also the appearance of the plateau between neighboring ODMPR peaks, the disappearance of ODMPR peaks, and changes in the ODMPR amplitude. For our numerical results of Eqs. (31), (35), and (36), GaAs-based superlattice and Ge-based superlattice will be used as a polar material and a nonpolar material, respectively. The used parameters which are the same as those used in the bulk semiconductors, have been utilized except for the electron density $n_e = 4\times10^{21}\,\mathrm{m}^{-3}$ and $d_{SL} = 9.93$ nm. In addition, as many as 21 Landau levels are included in the calculation of the

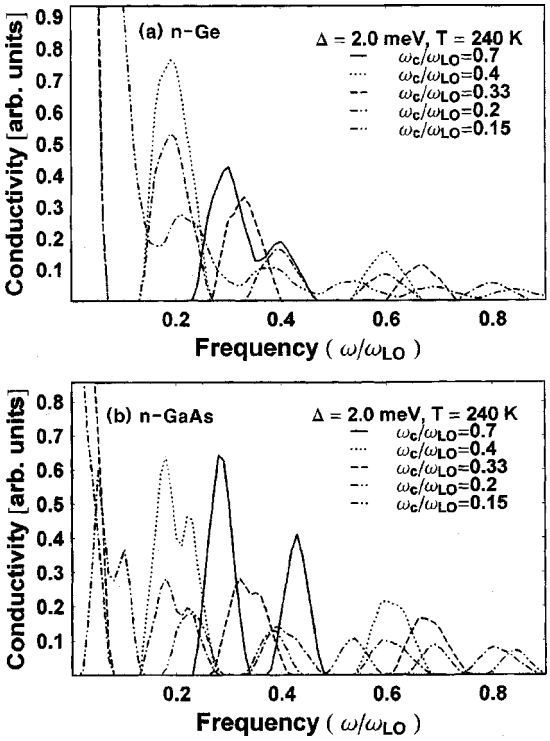

FIG. 5. Magnetic-field dependence of the magnetoconductivity $[\sigma_{zz}(\bar{\omega})]$ as a function of incident photon frequency for (a) Ge-based and (b) GaAs-based superlattices at $T=240$ K and $\Delta=2.0$ meV. The solid, dotted, dashed, dashed-dotted, and dashed-double dotted lines are, respectively, for $\omega_c/\omega_{LO}=0.7$, 0.4, 0.33, 0.2, and 0.15.

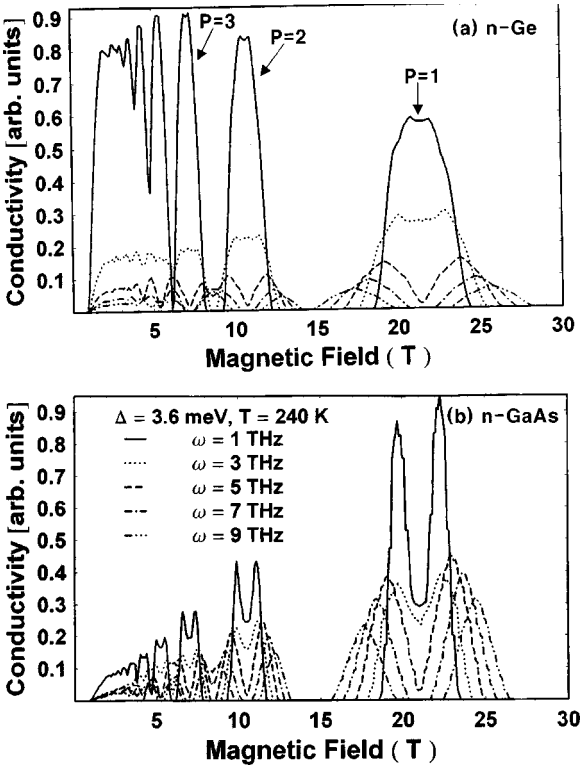

FIG. 6. Photon frequency dependence of the magnetoconductivity $[\sigma_{zz}(\bar{\omega})]$ as a function of applied magnetic field for (a) Ge-based and (b) GaAs-based superlattices at $T=240$ K and $\Delta=3.6$ meV. The solid, dotted, dashed, dashed-dotted, and dashed-double dotted lines are for $\omega=1$,3,5,7, and 9 THz, respectively. $P(\equiv N'-N=1,2,3,\ldots,)$ means the difference between two different Landau levels.

frequency-dependent magnetoconductivity. The sample temperature is assumed to be 240 K in this calculation of the longitudinal magnetoconductivity.

Figures 5(a) and 5(b) show the magnetic-field strength dependence of the magnetoconductivities $\sigma_{zz}(\bar{\omega})$ for Ge-based superlattice and GaAs-based superlattice, respectively, as a function of incident photon frequency, where a miniband width of $\Delta=2.0$ meV is taken as an example. Various peaks are observed according to the incident photon frequency and the strength of the magnetic field. It is clearly seen from the figures that all peaks are observed in terms of the optically detected magnetophonon resonance condition given by $P\hbar\omega_c=\hbar\omega_{LO}\pm\hbar\omega(P\equiv N'-N=1,2,3,\ldots,)$ and they can be assigned from the ODMPR condition. The remarkable thing here is that the positions of the ODMPR peaks are independent of the miniband width, but they are sensitive to the difference of Landau-level indices, the strength of applied magnetic field, LO phonon energy, and the photon energy.

Figure 6 shows the incident photon frequency dependence of the magnetoconductivities $\sigma_{zz}(\bar{\omega})$ for (a) Ge-based superlattice and (b) GaAs-based superlattice, respectively, as a function of magnetic field B at $T=240$ K, where various incident photon frequencies ranging from 1 THz to 9 THz are taken in order to investigate the dependence of the ODMPR effect on the incident photon frequency parameters. It is clearly seen from the figure that various peaks are observed according to the incident photon frequency. In these figures, we can see the following features: (i) the plateau between two neighboring peaks is clearly shown and is influenced by the incident photon frequency, (ii) the reduction in the ODMPR amplitude is observed as the incident photon frequency is increased, (iii) unlike low magnetic-field side, clear peaks arising from the optically detected magnetophonon resonance are observed in high magnetic-field side, (iv) as a linearly polarized photon of amplitude E and frequency ω is incident perpendicular to the z axis, the splitting of the ODMPR peaks takes place from the MPR peaks appearing in the absence of incident photon, (v) as the photon frequency is increased, the shifts of the ODMPR peak positions are increased, and (vi) as the difference of Landau-level indices is increased, the MPR and ODMPR peak positions are shifted to the lower magnetic-field side. It is to be noted that all features are the same for Ge-based superlattice and GaAs-based superlattice. Features (i) and (ii) can be readily understood from the plateau condition given by Eq. (40) and from the $\hbar\omega$ term in the denominator of Eq. (31), respectively.

Let us now address the reason why clear peaks are exhibited in high magnetic-field side unlike low magnetic-field side, which is related to feature (iii). The reason clear resonant peaks in the conductivity appear can be understood from the dispersion relation, the density of states of the su-

perlattice, and Eq. (40). In the case where the miniband width and the applied magnetic field are large enough and a minigap exists between two minibands, the DOS in the minibands do not overlap each other. However, if the strength of applied magnetic field is decreased, the energy separation between two Landau levels will decrease. As a consequence, the minigap between two neighboring minibands will disappear and the DOS will overlap. When the DOS in the minibands overlaps, numerous electron: LO-phonon interactions are expected under the condition of Eq. (40). Actually, clear peaks in the magnetoconductivity will disappear as in the low magnetic-field side. On the contrary, if the width of the miniband is sufficiently small, the minigap between two neighboring minibands will be very large under high magnetic fields. In this case, the minigap between two minibands will be very large and the DOS in the minibands will never overlap each other. The remarkable thing is that the DOS in the minibands begin to overlap in lower magnetic fields than in the large miniband case. Thus, when the miniband width is small, many peaks appear, whereas the number of peaks decreases with increasing miniband width. This feature—that the width of the ODMPR is better resolved as the miniband width decreases—can also be explained by Eq. (40), as Noguchi *et al.*[10] and Gassot *et al.*[12] did in detail. All these features are in good agreement with the experimental results of Noguchi *et al.*[10] and Gassot *et al.*[12] and with the theoretical results of Shu and Lei.[11]

The features (iv), (v), and (vi) can be readily understood from the condition for the ODMPR to give the peak positions (i.e., resonant magnetic fields) in the spectral line shape, which are mainly determined by the conditions $\Theta_{\nu,\pm}(k_z)=0$ and the arguments $a^2_{\nu,\pm}=0$ in Eqs. (35) and (36). The resonant behaviors are actually given by $P\hbar\omega_c = \hbar\omega_{LO} \pm \hbar\omega$ ($P \equiv N'-N = 1,2,3,\ldots,$). If there is no photon energy $\hbar\omega$ in the ODMPR condition, it becomes the MPR condition given by $P\hbar\omega_c = \hbar\omega_{LO}$ ($P \equiv N'-N = 1,2,3,\ldots$). Accordingly, we see that the ODMPR peaks are split from the MPR peaks. It seems that this splitting is due to the absorption and emission of a photon during the absorption of a phonon, and it is due to the incident photon being linearly polarized because the linearly polarized wave is composed of the superposition of a right-circularly polarized wave and a left-circularly polarized wave. For a fixed phonon energy in the ODMPR condition, as the photon frequency ω is increased, the shift of the resonant magnetic field (via ω_c) is increased, as in feature (v). In addition, for a fixed photon energy and a fixed phonon energy, the resonant magnetic field is decreased since $P\omega_c$ is constant if the difference in the Landau-level indices is increased, as in feature (vi). Thus it is to be noted that all features (iv), (v), and (vi) shown in Fig. 6 can be understood from the ODMPR condition.

Figure 7 shows the miniband width dependence of magnetoconductivity at $T=240$ K for $\omega=7$ THz as a function of the magnetic field, where two miniband widths are taken by 3.6 meV and 5.7 meV, respectively. It is clearly seen from the figures that the number of peaks varies with the miniband width, and that the plateaulike features and the heights of ODMPR peaks are very sensitive to the miniband width Δ.

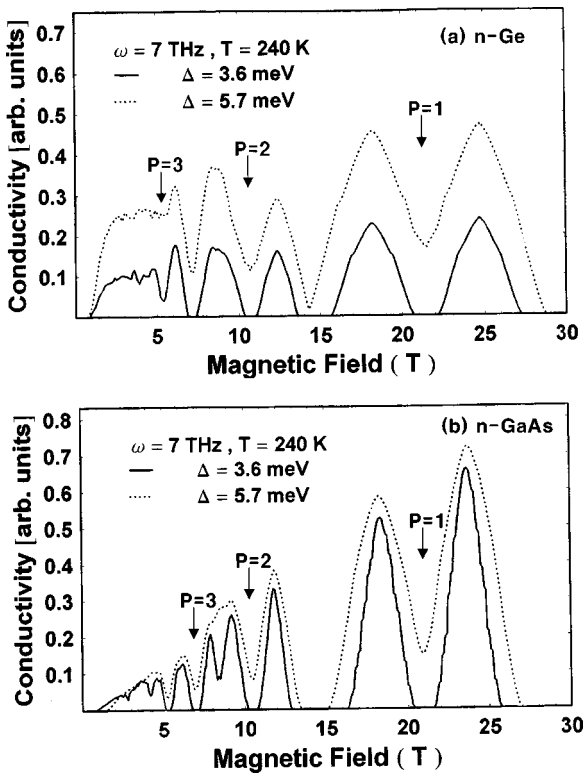

FIG. 7. Miniband-width dependence of the magnetoconductivity $[\sigma_{zz}(\bar{\omega})]$ at $T=240$ K and $\omega=7$ THz. The solid and dotted lines are for $\Delta=3.6$ meV and 5.7 meV, respectively. $P(\equiv N'-N = 1,2,3,\ldots,)$ means the difference between two different Landau levels.

The number of resonance peaks decreases with the increasing miniband width, whereas the amplitude of the resonance peaks increases with increasing miniband width. In addition, if the strength of the magnetic field is small, the amplitude of the resonance peak gets smaller. This can be understood by considering the relaxation rate, as pointed out by Noguchi *et al.*; when the Landau energy $\hbar\omega_c$ is small, the minigap disappears. In such a condition, the resonant feature of the relaxation rate becomes weak since the DOS of the minibands broaden and overlap, resulting in a reduction of the peaked feature. Hence, discrete features of the DOS are essential for observing clear resonance peaks.

IV. SUMMARY

So far, we have applied the frequency-dependent magnetoconductivity $\sigma_{yy}(\bar{\omega})$ and $\sigma_{zz}(\bar{\omega})$ obtained by using the Mori-type projection operator technique presented by one of the present authors[16] both to *n*-Ge and *n*-GaAs materials and to Ge-based and GaAs-based superlattices, and obtained the ODMPR conditions and an energy range in which the relaxation rates are allowed. With the ODMPR conditions and the obtained energy range, we have investigated the physical characteristics of the ODMPR effects in such bulk semiconductors and semiconductor superlattices.

In the bulk semiconductors and the semicoductor superlattices, particularly, we have studied the anomalous behav-

ior of the ODMPR line shape, such as the splitting and the shift of ODMPR.

Our results for the bulk semiconductors show a linearly polarized photon of amplitude E and frequency ω along the z axis, and our results for the semiconductor superlattices show a linearly polarized photon of amplitude E and frequency ω perpendicular to the z axis, but they both show the same results as follows:(1) the splitting of the ODMPR peaks takes place from the MPR peaks, (2) as the photon frequency is increased, the shifts of the ODMPR peak positions are increased, (3) as the difference of Landau-level indices is increased, the MPR and ODMPR peak positions are shifted to the lower magnetic-field side, and (4) the shifts of ODMPR are increased as the incident photon frequency is increased and the difference in the Landau-level indices is decreased.

Our results for the semiconductor superlattices only show that (5) the plateau between two neighboring peaks is clearly shown and is influenced by the incident photon frequency, (6) the reduction in the ODMPR amplitude is observed as the incident photon frequency is increased, and (7) unlike low magnetic-field side, clear peaks arising from the optically detected magnetophonon resonance are observed in high magnetic-field side.

In addition, strong oscillations of the magnetoconductivity both in bulk materials such as n-Ge and $n-$GaAs, and in Ge-based and GaAs-based superlattices are expected in terms of the optically detected magnetophonon resonance, which indicate that the ODMPR should also be observed experimentally in such bulk semiconductors, as pointed out by Hai and Peeters.[14]

Some comments related to this work should be made: The single-particle picture has been used throughout this work; thus electron-electron interactions have been ignored. The effect of electron-electron interactions can be taken into account approximately by replacing the electron-phonon interaction $C(\mathbf{q})$ with a screened electron-phonon interaction $C(\mathbf{q})=iD\hbar^{1/2}/(2\rho\omega_{LO}\Omega)^{1/2}(1+\lambda^2(\mathbf{q})/q^2)^7$ because the inverse screening length $\lambda(\mathbf{q})$ depends on the electron density n_e, which in general depends on the temperature T and the magnetic field $\mathbf{B}$. Therefore, we would expect the screening to be significant only if the electron density n_e exceeded a critical value $n_{cr}(T,\mathbf{B})$. In that case, the effects of electron-electron scattering would be significant, the relaxation rate would be changed, and the temperature dependence of the heights of the ODMPR peaks would be affected by electron-electron scattering.

In addition, the influence of spin splitting has been neglected. Despite the above shortcomings of the theory, we believe that our results make it possible to understand analytically the essential physics of ODMPR in bulk materials such as n-Ge and $n-$GaAs, and in Ge-based and GaAs-based superlattices with nonpolar and polar properties, respectively.

ACKNOWLEDGMENTS

This research was supported by the Korea Science and Engineering Foundation (KOSEF Grant No. 2001-1-11400-010-3).

[1] V.L. Gurevich and Yu A. Firsov, Zh. Éksp. Teor. Fiz. **40**, 198 (1961) [Sov. Phys. JETP **13**, 137 (1961)].
[2] R.J. Nicholas, Prog. Quantum Electron. **10**, 1 (1985).
[3] D. Schneider, C. Brink, G. Irmer, and P. Verma, Physica B **256-258**, 625 (1998); D. Schneider, K. Pricke, J. Schulz, G. Irmer, and M. Wenzel, in *Proceedings of the 23rd International Conference on the Physics of Semiconductors*, edited by M. Scheffler and R. Zimmermann (World Scientific, Singapore, 1996), p. 221.
[4] P. Warmenbol, F.M. Peeters, and J.T. Devreese, Phys. Rev. B **39**, 7821 (1989); **37**, 4694 (1988).
[5] N. Mori, H. Momose, and Hamaguchi, Phys. Rev. B **45**, 4536 (1992).
[6] J.Y. Ryu and R.F. O'Connell, Phys. Rev. B **48**, 9126 (1993); J.Y. Ryu, G.Y. Hu, and R.F. O'Connell, Phys. Rev. B **49**, 10 437 (1994).
[7] A. Suzuki and M. Ogawa, J. Phys. C **10**, 4659 (1998).
[8] G. Ploner, J. Smoliner, G. Strasser, M. Hauser, and E. Gornik, Phys. Rev. B **57**, 3966 (1998).
[9] S.C. Lee, J.Y. Ryu, S.W. Kim, and C.S. Ting, Phys. Rev. B **62**, 5045 (2000).
[10] H. Noguchi, H. Sakaki, T. Takamasu, and N. Miura, Phys. Rev. B **45**, 12 148 (1992).
[11] W.M. Shu and X.L. Lei, Phys. Rev. B **50**, 17 378 (1994).
[12] P. Gassot, J. Genoe, D.K. Maude, J.C. Portal, K.S.H. Dalton, D.M. Symons, R.J. Nicholas, F. Aristone, J.F. Palmier, and F. Laruelle, Phys. Rev. B **54**, 14 540 (1996).
[13] S.C. Lee, D.S. Kang, J.D. Ko, Y.H. Yu, J.Y. Ryu, and S.W. Kim, J. Korean Phys. Soc. **39**, 643 (2001).
[14] G.-Q. Hai and F.M. Peeters, Phys. Rev. B **60**, 16 513 (1999).
[15] D.J. Barnes, R.J. Nicholas, F.M. Peeters, X.G. Wu, J.T. Devreese, J. Singleton, C.J.G.M. Langerak, J.J. Haris, and C. T. Foxon, Phys. Rev. Lett. **66**, 794 (1991).
[16] J.Y. Ryu, Y.C. Chung, and S.D. Choi, Phys. Rev. B **32**, 7769 (1985); J.Y. Ryu and S.D. Choi, Prog. Theor. Phys. **72**, 429 (1984); J. Y. Ryu, Ph.D. thesis (Kyungpook National University, 1989) (unpublished).
[17] S.D. Choi and O.H. Chung, Solid State Commun. **46**, 717 (1983).
[18] P.N. Argyres and J.L. Sigel, Phys. Rev. B **10**, 1139 (1974).
[19] I. S. Gradshteyn and I. M. Ryzhik, *Tables of Integrals, Series and Products* (Academic, New York, 1965).
[20] J. Singh, *Physics of Semiconductors and Their Heterostructures* (McGraw-Hill, Singapore, 1993), p. 455.
[21] B. K. Ridley, *Quantum Processes in Semiconductors* (Clarendon Press, Oxford, 1993), p. 256.